Korean Chem. Eng. Res., 64(1), 105152 (2026)
https://doi.org/10.9713/kcer.2026.64.1.105152
PISSN 0304-128X, EISSN 2233-9558

Direct Synthesis of Hydrogen Peroxide over Pd Catalysts Supported on Glucose-derived N-doped Carbons: Effect of Nitrogen Doping on Catalytic Activity

Seung-Yeol Oh‡, Na-Yeong Ahn‡ and Young-Min Chung†

Department of Chemical Engineering, Kunsan National University, 558 Daehak-ro, Gunsan, Jeollabuk-do, 54150, Korea
(Received 19 December 2025; Received in revised from 14 January 2026; Accepted 15 January 2026)

Abstract – Nitrogen-doped porous carbons (CN_x) were prepared from glucose-derived hydrochar via hydrothermal treatment followed by chemical activation with melamine, and then used as supports for Pd catalysts (Pd/CN_x, where x denotes the N content in wt%) for the direct synthesis of H_2O_2 from H_2 and O_2 (DSHP). Optimal N doping played an important role in increasing the surface area and the density of pyridinic/pyrrolic sites in CN_x, thereby improving Pd dispersion and reducing the mean Pd nanoparticle size. Among the Pd/CN_x catalysts tested, $Pd/CN_{0.8}$ exhibited the best performance, achieving 91% H_2O_2 selectivity and a productivity of 7056 mmol H_2O_2/g-Pd·h at 39% H_2 conversion. In contrast, $Pd/CN_{1.4}$ and $Pd/CN_{8.5}$ showed sharply decreased H_2O_2 selectivity and productivity due to accelerated H_2O_2 hydrogenation and decomposition over these catalysts. These results clearly demonstrate the importance of an optimal N-doping level for achieving high H_2O_2 selectivity and productivity in the DSHP reaction over Pd/CN_x catalysts.

Key words: Direct synthesis of H_2O_2, N-doped carbon, Chemical activation, Supported Pd catalyst

1. Introduction

Hydrogen peroxide (H_2O_2) is a widely used oxidant in various industrial fields, including pulp and textile bleaching, wastewater treatment, semiconductor cleaning, and fine chemical synthesis. Since water is the only by-product formed during its decomposition or hydrogenation, H_2O_2 has attracted great attention as an environmentally benign oxidizing agent. Currently, most of industrial H_2O_2 production depends on the anthraquinone oxidation (AO) process, which involves multi-step, energy-intensive reactions, the use of toxic organic solvents, and the generation of a significant amount of waste. In addition, to ensure economic efficiency, H_2O_2 must be produced and transported in highly concentrated forms, which causes major safety concerns [1]. As an alternative to address these problems, the direct synthesis of hydrogen peroxide (DSHP) from hydrogen and oxygen has emerged as a promising solution [2-4]. The DSHP process offers a simple reaction pathway and high atom utilization efficiency and enables safe on-site production of H_2O_2 at low concentrations when needed [2,3].

However, achieving high H_2O_2 selectivity remains challenging due to thermodynamic limitations and the explosion risk of H_2/O_2 mixtures [2,4]. In DSHP, both the desired formation of hydrogen peroxide and side reactions such as water formation, hydrogenation, and decomposition of H_2O_2 occur simultaneously on the same active metal sites, such as palladium (Pd), and these side reactions are thermodynamically more favorable (Scheme 1) [5–8]. Moreover, to avoid the risk of explosion, the hydrogen concentration in the reactor must be kept below a threshold, which reduces the overall H_2 availability during the reaction and leads to low H_2O_2 yield [2,4]. To suppress these side reactions, the addition of acids or halide promoters has been proposed [9–12], but such additives can cause corrosion and environmental issues, making them unsuitable for sustainable processes [13].

Among many catalysts studied for DSHP, palladium supported on carbon (Pd/C) is widely used due to its low cost and chemical stability [2,4,14]. However, the catalytic performance of Pd/C is strongly influenced by complex factors such as the size and dispersion of Pd nanoparticles (NPs), their electronic state, the surface chemistry and pore structure of the carbon support, and the hydrophilic/hydrophobic nature of the catalyst [15–20]. Therefore, precisely controlling the physicochemical properties of both the active metal and the support is crucial for developing efficient and selective catalysts [16,17,21,22].

In this context, carbon supports doped with nitrogen (N) heteroatoms have recently gained significant attention [13,23,24]. N-doping can create electron-rich sites that promote the uniform dispersion of Pd NPs and modulate their electronic interaction with the support [13,23–

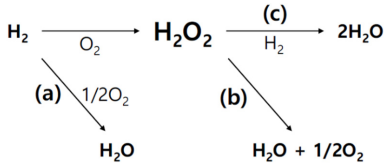

Scheme 1. Reaction pathways in the direct synthesis of hydrogen peroxide (DSHP): (a) direct oxidation of H_2O, (b) H_2O_2 decomposition, and (c) H_2O_2 hydrogenation.

† To whom correspondence should be addressed.
E-mail: ymchung@kunsan.ac.kr
‡ Equal contribution

25]. Moreover, different types of nitrogen species (*e.g.,* graphitic-N, pyridinic-N, and pyrrolic-N) influence the electronic structure of Pd and the reaction pathways in distinct ways, ultimately contributing to the improved selectivity and productivity of H_2O_2 [23,25–27]. To modify the carbon structure, potassium hydroxide (KOH) has been commonly used as a chemical activating agent due to its ability to produce high surface area and microporosity [28,29]. However, KOH is highly corrosive and toxic, causing serious environmental concerns during both the preparation and post-treatment processes. In particular, activated carbon produced using KOH requires extensive washing with strong acids (typically HCl) to remove residual KOH and by-products, generating a large amount of hazardous wastewater [28]. In this study, a more environmentally benign activation approach was adopted by replacing KOH with potassium carbonate (K_2CO_3) and potassium chloride (KCl). K_2CO_3 is a milder inorganic base with significantly lower environmental risks, while KCl acts as a salt-templating agent that induces porosity through physical behavior and can be removed easily by water washing. The combined use of K_2CO_3 and KCl enables simultaneous chemical activation and physical templating, resulting in high surface area and uniform porous structure. Furthermore, since the resulting residues are highly water-soluble, post-treatment can be achieved by simple rinsing with water without the need for acid washing [28,29].

Before chemical activation, hydrochar was prepared via hydrothermal synthesis using glucose as a carbon source and then activated with a K_2CO_3–KCl system for the preparation of nitrogen-doped porous carbon supports [30]. By adjusting the amount of melamine as a nitrogen source, nitrogen-doped carbon (CN_x) with different nitrogen contents was obtained [23,25]. Palladium was subsequently deposited on the CN_x supports to form Pd/CN_x catalysts [15,18,31].

We systematically investigated how varying nitrogen content influences the support's physicochemical properties, the dispersion and electronic state of Pd NPs, and the catalytic performance of Pd/CN_x in DSHP. As discussed below, this work presents an example of a Pd/CN_x catalyst design achieving high H_2O_2 selectivity and productivity in DSHP.

2. Materials and Methods

2-1. Chemicals

D-Glucose ($C_6H_{12}O_6$), potassium tetrachloropalladate(II) (K_2PdCl_4), Cerium(IV) sulfate standard solution (0.25 N in 2–3 N sulfuric acid) and ferroin indicator ($[Fe(C_{12}C_8N_2)_3]SO_4$, 0.1 wt% in H_2O) were obtained from Sigma-Aldrich. Melamine ($C_3H_6N_6$), potassium chloride (KCl, 99.0%), methyl alcohol (CH_3OH, 99.8%) and hydrogen peroxide (H_2O_2, 34.5%) were supplied from Samchun Chemicals (Korea). Potassium carbonate (K_2CO_3, 99.5%) was purchased from Junsei Chemical. All the chemicals were used as-received without further purification.

2-2. Catalyst preparation

Hydrochar was synthesized via a hydrothermal reaction. For example, glucose and deionized water were placed into a Teflon-lined autoclave and heated at 473 K for 24 h. The resulting hydrochar was collected and used as a carbon precursor for nitrogen doping. Nitrogen-doped carbon supports (CN_x, where x = 0, 0.5, 0.8, 1.4, and 8.5) were prepared by mixing hydrochar, KCl, and K_2CO_3 in a mass ratio of 1:11:3, followed by adding varying amounts of melamine as the nitrogen source. The mixture was calcined at 1073 K for 1 h under an inert atmosphere in a tubular furnace (100 ml/min N_2). After natural cooling to room temperature, the calcined product was washed with ultrapure water, filtered, and dried in an oven at 353 K for 12 h.

The Pd/CN_x catalyst was prepared via incipient wetness impregnation method with the anionic palladium precursor K_2PdCl_4. Typically, pre-determined K_2PdCl_4 solution (Pd intake 1 wt%) was slowly dropped on the dried CN_x support with thorough mixing. After aging at 298 K for 12 h, the Pd impregnated sample was dried at 393 K for 12 h and finally calcined at 523 K for 3 h under air (100 mL/min). The resulting catalyst was denoted as Pd/CN_x.

2-3. Characterization

The textural properties of the N-doped carbon, *i.e.,* the specific surface area, pore volume, and pore diameter, were determined by N_2 adsorption using a BELSORP-MaxII (MicrotracBEL, Japan) at 77 K. The crystalline structure of Pd/CN_x was examined using powder X-ray diffraction (PXRD) patterns, obtained with a Rigaku SmartLab SE equipped with Cu Kα radiation (λ = 1.54 Å). The particle size distribution and the electronic properties of Pd NPs on Pd/CN_x were analyzed using transmission electron microscopy (TEM) and X-ray photoelectron spectroscopy (XPS), respectively. TEM analyses was conducted using a JEM-ARM200F (Jeol, Japan) at an acceleration voltage of 200 kV. XPS measurements were performed on an Axis Supra+ (Kratos Analytical, UK) with monochromatic Al Kα radiation at a pass energy of 40 eV. The binding energies of the chemical species were calibrated using the C 1s peak at 284.6 eV.

2-4. Direct synthesis, decomposition, and hydrogenation of H_2O_2

[Caution] H_2 and O_2 can form explosive mixtures over a very wide concentration range (4~75 vol% H_2 in air; 4~94 vol% in O_2). Therefore, the H_2 concentration must be diluted and maintained below 4 vol%. The direct synthesis of hydrogen peroxide from hydrogen and oxygen was carried out in a 100 mL jacked high-pressure reactor (Büchi Picoclave, Switzerland) connected to a circulator (F25-HE, Julabo, Germany). In a typical run, the catalyst (20 mg) was introduced to the reactor with 26 g of a methanol/water mixture (60 wt% methanol). The reactor was tightly closed, pressurized up to 5 bar with nitrogen in static mode, and evacuated to remove residual gases. The purging step was repeated three times. During the purging, the reaction temperature was adjusted to 275 K. After the purging process, the nitrogen gas in the reactor was replaced with reactant gases by co-feeding 5 mol% H_2/N_2 (30 mL/min) and 20 mol% O_2/N_2 (10 mL/min) to the reactor using two high pressure mass flow controllers (Brooks 5850E, Netherland), and the reactor was pressurized to 30 bar with the mixed

gases. After temperature and pressure were stabilized, a reaction run was initiated by stirring (1200 rpm) and maintained for 1 h. During the reaction, the mixed gases were continuously supplied to the reactor at a total flow rate of 40 mL/min ($H_2/O_2/N_2$ (mol%) = 3.8/5.0/91.2), and the reaction pressure was maintained using a back pressure regulator (BPR, Tescom, USA). At the end of the reaction run, the catalyst was carefully separated from the reaction product by filtration, washed thoroughly with methanol/water, and dried for further use. The amount of hydrogen peroxide produced was determined by titration with a cerium(IV) sulfate standard solution and ferroin indicator. To determine the change in hydrogen concentration during the reaction, the off-gas collected in a gas bag was analyzed with a gas chromatograph (GC, Agilent 6890N, USA) equipped with a Carboxen-1010 PLOT capillary column (30 m, 0.53 mm ID) and a thermal conductivity detector (TCD) using Ar as a carrier gas. Hydrogen conversion and selectivity were calculated according to the following equations using the hydrogen peroxide and hydrogen concentrations determined by the titration and GC analysis, respectively.

$$\text{Hydrogen Conversion (\%)} = \frac{\text{Moles of hydrogen reacted}}{\text{Moles of hydrogen supplied}} \times 100$$

$$\text{Hydrogen Selectivity (\%)} = \frac{\text{Moles of hydrogen peroxide produced}}{\text{Moles of hydrogen reacted}} \times 100$$

The hydrogen peroxide productivity is defined as the amount of hydrogen peroxide produced per hour divided by the Pd content (mmol H_2O_2/g-Pd·h). The hydrogen conversion was calculated as the ratio of the moles of hydrogen reacted to the moles of hydrogen supplied to the reactor, expressed as a percentage. The hydrogen peroxide selectivity was calculated as the ratio of the moles of hydrogen peroxide produced to the moles of hydrogen reacted, expressed as a percentage.

H_2O_2 decomposition and hydrogenation tests were conducted at 275 K under atmospheric pressure. For the H_2O_2 decomposition, the reaction solution consisted of 20 mg of catalyst and 50 g of mixed methanol/water solution containing 1 wt% H_2O_2 magnetically stirred for 1 h under nitrogen. H_2O_2 hydrogenation was carried out in a similar manner under bubbling H_2 (5 mL/min). The decomposed and hydrogenated hydrogen peroxide concentrations were also determined by titrating the reaction mixture.

3. Results and Discussion

3-1. Preparation of Pd/CN_x catalysts

The Pd/N-doped carbon (Pd/CN_x) catalysts were synthesized from glucose as the carbon precursor via a two-step process as described in Scheme 2. In the first step, hydrothermal carbonization of glucose at 473 K for 24 h produced hydrochar, in which most oxygen-containing surface groups were removed, yielding spherical amorphous carbon particles that provided a suitable platform for further modification [30]. In the second step, the hydrochar was mixed with melamine as the nitrogen source and K_2CO_3/KCl as chemical activators, followed by chemical activation at 1073 K. This step simultaneously generated a microporous structure and incorporated nitrogen species, introducing pyridinic, pyrrolic, and graphitic nitrogen sites into the carbon framework [25–27]. K_2CO_3 and KCl served as activating agents, producing a porous structure with high surface area and enhanced electronic properties [28,29]. The resulting N-doped carbon (CN_x) provided abundant nitrogen-coordination sites for noble metal anchoring [23,25,27]. Palladium was introduced via incipient wetness impregnation method by contacting CN_x with an anionic palladium precursor solution (K_2PdCl_4). Strong interactions between the nitrogen coordination sites and the $[PdCl_4]^{2-}$ ion enabled selective and uniform adsorption of Pd precursor on the N-doped sites [23,25]. Upon calcination, the adsorbed $[PdCl_4]^{2-}$ ion was reduced and converted into metallic Pd NPs. Nitrogen coordination effectively suppressed particle aggregation, strengthened metal–support interactions, and optimized the Pd electronic structure [23,32].

Fig. 1(a) shows the changes in the surface area and actual nitrogen content of N-doped carbons (CN_x). The nitrogen content increased gradually from CN_0 to $CN_{1.4}$, followed by a sharp rise to over 8 wt% for $CN_{8.5}$. In contrast, the surface area increased almost linearly from

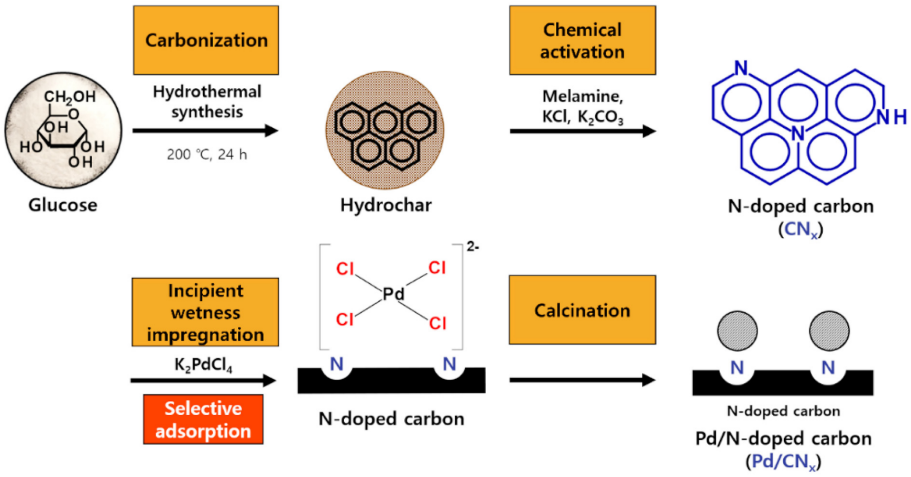

Scheme 2. Preparation of Pd/N-doped carbons (Pd/CN_x) with different nitrogen contents.

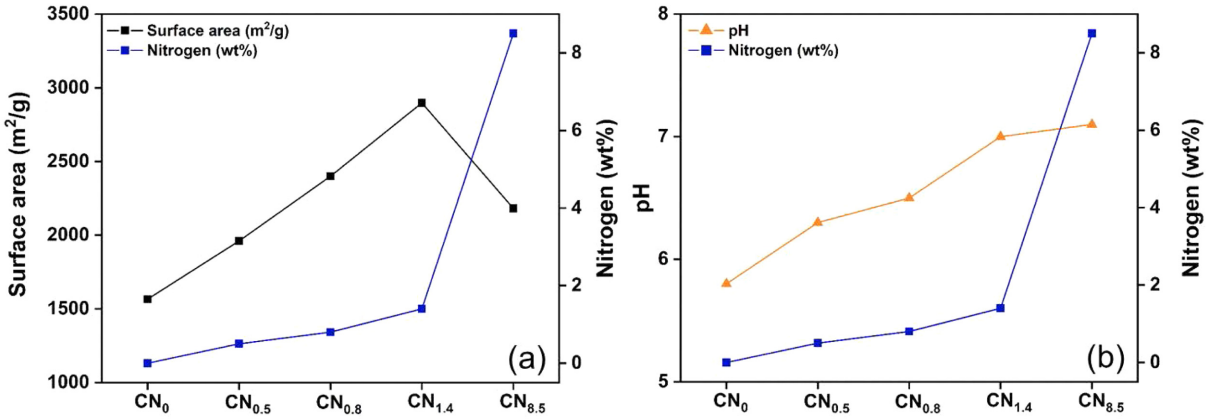

Fig. 1. (a) Changes in the surface area and N content of CN_x and (b) effect of N content in CN_x on the pH of the MeOH/H_2O reaction solution.

about 1,550 m^2/g for CN_0 to approximately 2,900 m^2/g for $CN_{1.4}$, after which it decreased markedly to around 2,300 m^2/g for $CN_{8.5}$. The volcano-shaped relationship between nitrogen content and surface area of CN_x suggests that nitrogen doping promotes pore structure development and surface area enhancement up to an optimal level, beyond which excessive nitrogen incorporation leads to pore structure collapse and a subsequent reduction in surface area [29].

The relationship between nitrogen content and the pH of the MeOH/H_2O reaction solution is presented in Fig. 1(b). As the nitrogen content increased, the pH shifted from near-neutral toward a more basic range [25]. However, even with the highest nitrogen content ($CN_{8.5}$), the pH did not increase significantly compared to $CN_{1.4}$ suggesting that the weakly basic nitrogen species on the carbon surface contribute only modestly to the pH increase.

In Fig. 2 and Table 1, the textural properties of the N-doped carbons characterized by N_2 adsorption–desorption and elemental analyses are presented. The results indicate that all CN_x samples possessed a predominantly microporous structure regardless of nitrogen content. The specific surface area and total pore volume increased steadily up to $CN_{1.4}$, suggesting enhanced pore development with moderate nitrogen doping. However, a noticeable decrease was observed for $CN_{8.5}$, likely due to partial pore blockage or collapse at excessive nitrogen loadings. In contrast, the average pore size remained essentially unchanged, implying that nitrogen doping primarily affects the pore accessibility rather than altering the intrinsic pore dimensions. Consistently, the pore-size distributions (Fig. 2(b)) are dominated by micropores (< 2 nm) for all CN_x, while the mesopore contribution remains minor and becomes slightly more pronounced up to $CN_{1.4}$ but attenuates for

Table 1. Physico-chemical properties of CN_x

Sample	Surface area (m^2/g)	Pore volume (cm^3/g)	Pore diameter (nm)	Elemental analysis (%)		
				C	H	N
CN_0	1,566	0.9	2.2	-	-	-
$CN_{0.5}$	1,961	1.1	2.2	92.5	0.23	0.5
$CN_{0.8}$	2,404	1.3	2.1	92.5	0.24	0.8
$CN_{1.4}$	2,898	1.6	2.2	92.9	0.2	1.4
$CN_{8.5}$	2,183	1.2	2.2	78.3	0.8	8.5

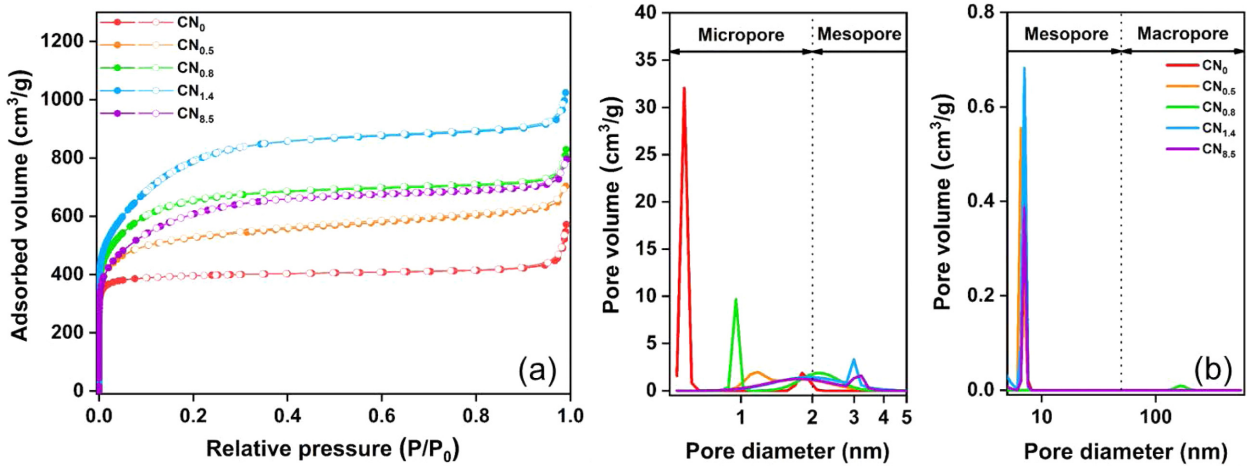

Fig. 2. (a) Nitrogen adsorption–desorption isotherms and (b) pore size distribution of CN_x.

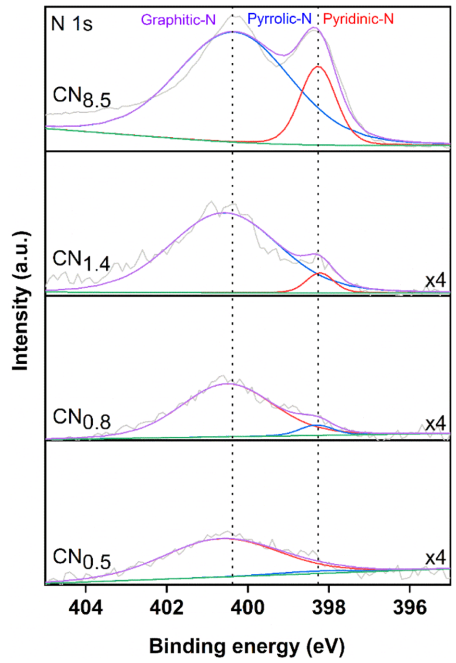

Fig. 3. N 1s XPS spectra of CN_x.

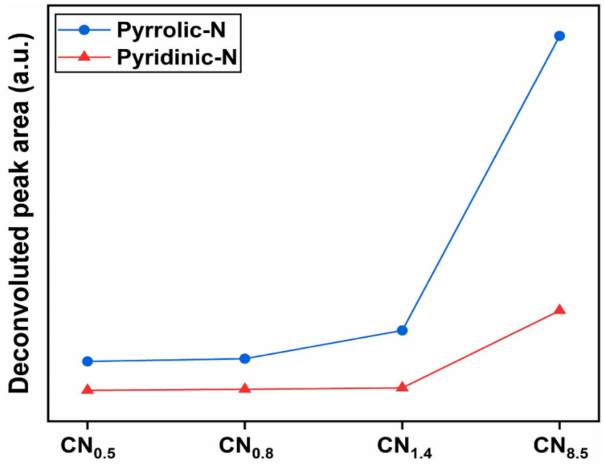

Fig. 4. XPS-derived pyrrolic-N and pyridinic-N contents in CN_x.

$CN_{8.5}$. Table 1 summarizes the textural parameters and compositional analysis of the CN_x series.

In the XRD patterns (Fig. 5), the characteristic reflections of metallic Pd, assigned to the (111) and (200) planes, were observed at approximately $2\theta \approx 40°$ and $\approx 46°$, respectively. Notably, the intensities of these Pd reflections decrease systematically as the nitrogen content increases from CN_0 to $CN_{8.5}$. This trend suggests that nitrogen doping alters the crystallinity or coherent domain size of Pd and potentially its dispersion state, implying that Pd may be present as relatively smaller crystalline domains (or in a more highly dispersed form) at higher N loadings.

This interpretation is consistent with the TEM observations (Fig. 6). The mean Pd NP size for Pd/CN_0 is 2.62±1.19 nm with a broad distribution, whereas $Pd/CN_{0.5}$, $Pd/CN_{0.8}$, and $Pd/CN_{1.4}$ exhibit smaller average sizes of 2.12±0.51 nm, 2.12±0.56 nm, and 2.10±0.75 nm,

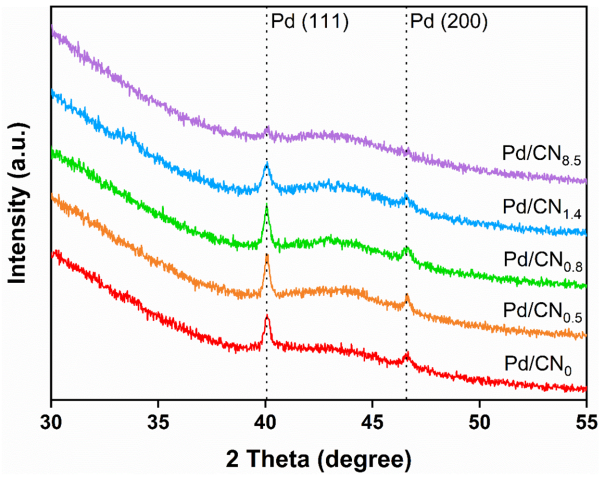

Fig. 5. XRD patterns of Pd/CN_x.

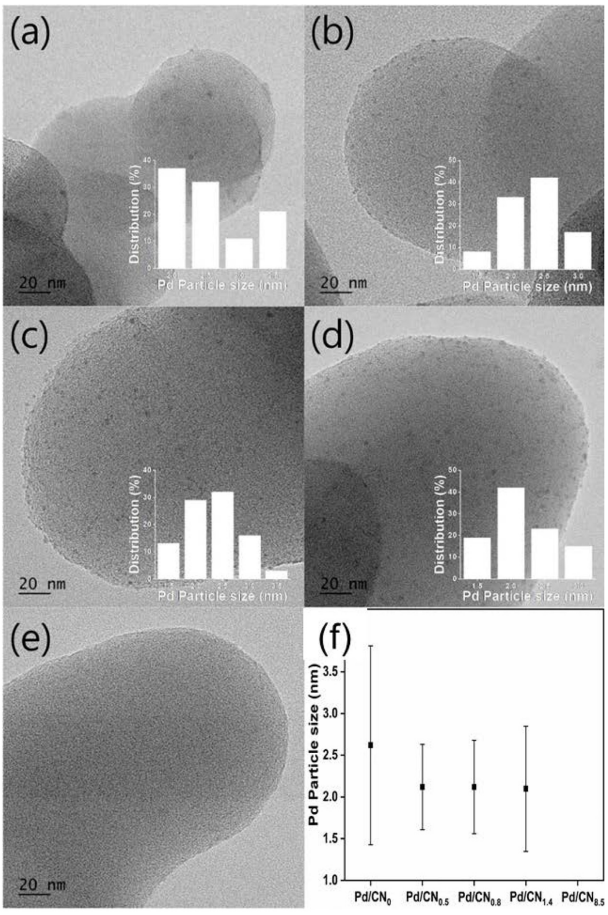

Fig. 6. TEM images of Pd/CN_x catalysts and their Pd NP size distributions: (a) Pd/CN_0, (b) $Pd/CN_{0.5}$, (c) $Pd/CN_{0.8}$, (d) $Pd/CN_{1.4}$, (e) $Pd/CN_{8.5}$, and (f) Pd NP size distributions.

respectively, together with comparatively narrower size distributions. These results imply that increased nitrogen functionalities influence Pd precursor immobilization and nucleation behavior on the carbon surface, thereby suppressing particle growth . For $Pd/CN_{8.5}$, distinct Pd NPs are not clearly resolved in TEM, which may indicate that Pd exists as extremely small clusters or a highly dispersed species that is

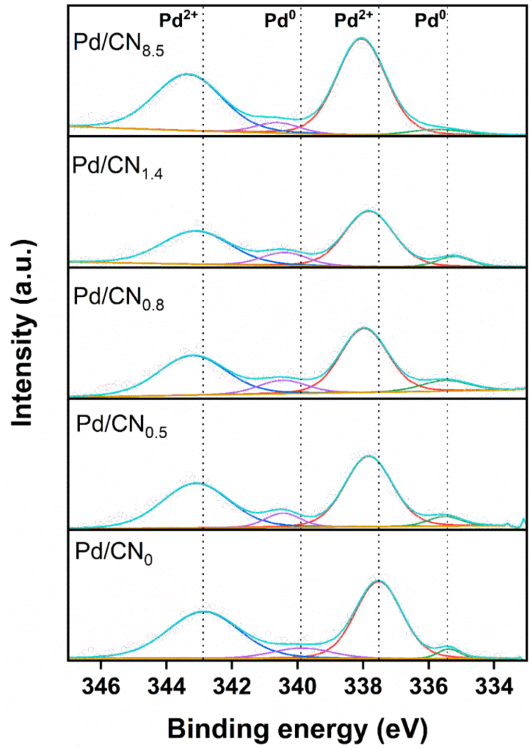

Fig. 7. Pd 3d XPS spectra of Pd/CN$_x$ catalysts.

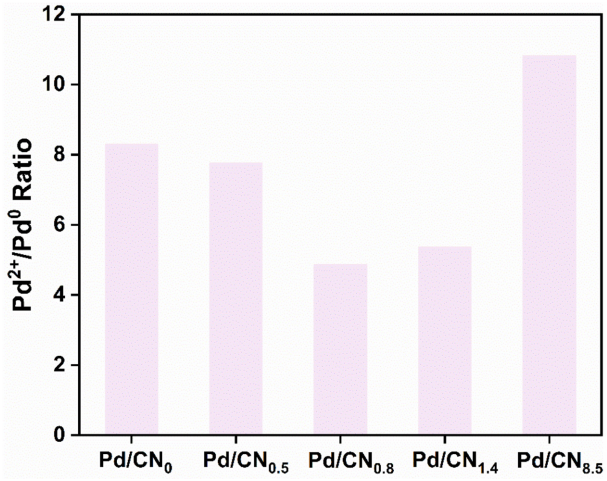

Fig. 8. Pd^{2+}/Pd^0 ratio of Pd/CN$_x$.

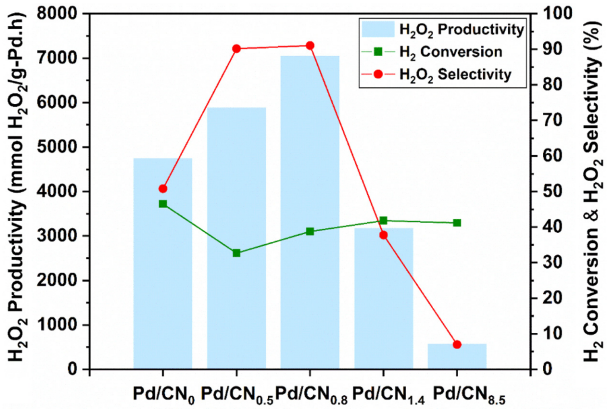

Fig. 9. Direct synthesis of H_2O_2 over Pd/CN$_x$ catalysts. Reaction conditions: catalyst (20 mg), $N_2/H_2/O_2$ (mol%)=3.8/5.0/91.2 (30 bar), total gas flow rate=40 mL/min, 60 wt% methanol/water solvent (26 g), 275 K, 1 h.

difficult to distinguish under the present imaging conditions.

The Pd 3d XPS spectra of the Pd/CN$_x$ catalysts shown in Fig. 7 indicate the coexistence of Pd^0 and Pd^{2+} species showing that Pd^{2+} is predominant across the entire series. The corresponding Pd^{2+}/Pd^0 ratios derived from the fitted components are summarized in Fig. 8, highlighting that the surface Pd is largely present in an oxidized state on all CN$_x$ supports. This implies that the accessible Pd sites are more plausibly described as a mixed Pd^{2+}/Pd^0 surface rather than a purely metallic phase. Such a mixed oxidation state is particularly relevant to DSHP, because the Pd^{2+}/Pd^0 balance can modulate not only H_2/O_2 adsorption, but also the susceptibility of the freshly formed H_2O_2 to non-selective consumption pathways such as hydrogenation and decomposition as described in Scheme 1 [7,9,23].

Moreover, as the nitrogen content increases, both the Pd^0 and Pd^{2+} components in Fig. 7 exhibit a slight shift toward higher binding energies. This trend is qualitatively consistent with an altered local electronic environment around Pd arising from interactions with N functionalities and/or with the relative stabilization of oxidized Pd species [23,32]. These results suggest that the N-doping level can tune the Pd oxidation state (and the Pd^{2+}/Pd^0 balance), thereby influencing the selectivity and productivity of the DSHP reaction.

3-2. Direct synthesis of H_2O_2

Fig. 9 shows that the reaction performance of Pd/CN$_x$ catalysts such as H_2O_2 productivity strongly depends on the H_2O_2 selectivity rather than H_2 conversion. Pd/CN$_0$ exhibits a high H_2 conversion of 47%, but its selectivity remains at 51%, leading to a limited productivity of 4750 mmol H_2O_2/g-Pd·h. In contrast, for Pd/CN$_{0.5}$ and Pd/CN$_{0.8}$, although the H_2 conversion does not increase monotonically (33% and 39%, respectively), the selectivity markedly improves to 90–91%, resulting in higher productivities of 5892–7056 mmol H_2O_2/g-Pd·h. Conversely, Pd/CN$_{1.4}$ and Pd/CN$_{8.5}$ maintain H_2 conversions in the ~41% range, yet their selectivity sharply drop to 38% and 7%, causing the productivities to decrease substantially to 3177 and 575 mmol H_2O_2/g-Pd·h, respectively. This trend is consistently supported by the H_2O_2 decomposition and hydrogenation results shown in Fig. 10. The highly selective and productive CN$_{0.5}$–CN$_{0.8}$ catalysts exhibit only minor changes in H_2O_2 concentration over time in both tests, indicating that the generated H_2O_2 is relatively stable. In contrast, CN$_{1.4}$ and especially CN$_{8.5}$ show pronounced H_2O_2 consumption, suggesting that under DSHP conditions the generated H_2O_2 is likely to be rapidly depleted via decomposition or hydrogenation before it can accumulate.

3-3. Catalyst recycle test

Fig. 11(a) presents the recyclability of the Pd/CN$_{0.8}$ catalyst under DSHP condition. The H_2 conversion remains relatively stable, decreasing

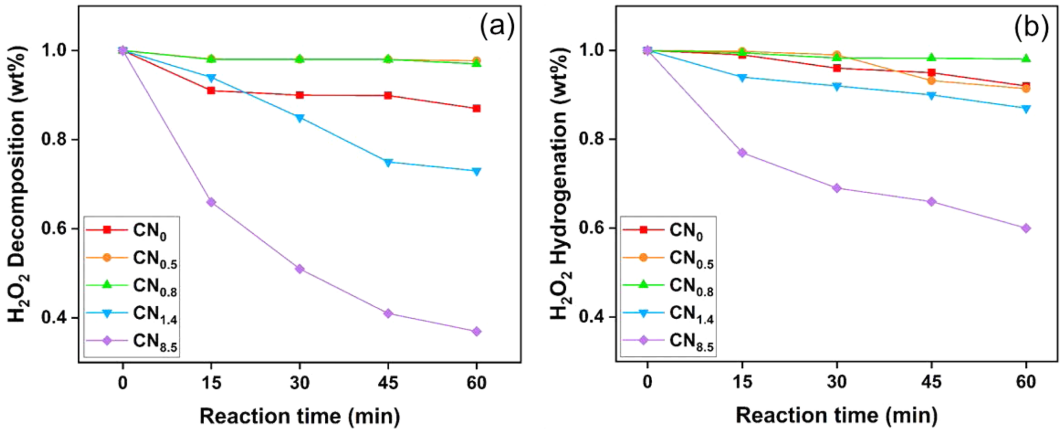

Fig. 10. (a) H_2O_2 decomposition and (b) H_2O_2 hydrogenation over Pd/CN_x catalysts. Reaction conditions: catalyst (20 mg), 1 wt% H_2O_2 in 60 wt% methanol/water solvent (50 g), 1 bar, 275 K, 1 h. Gas flow rate for H_2O_2 decomposition = 5 mL/min (N_2). Gas flow rate for H_2O_2 hydrogenation = 5 mL/min.

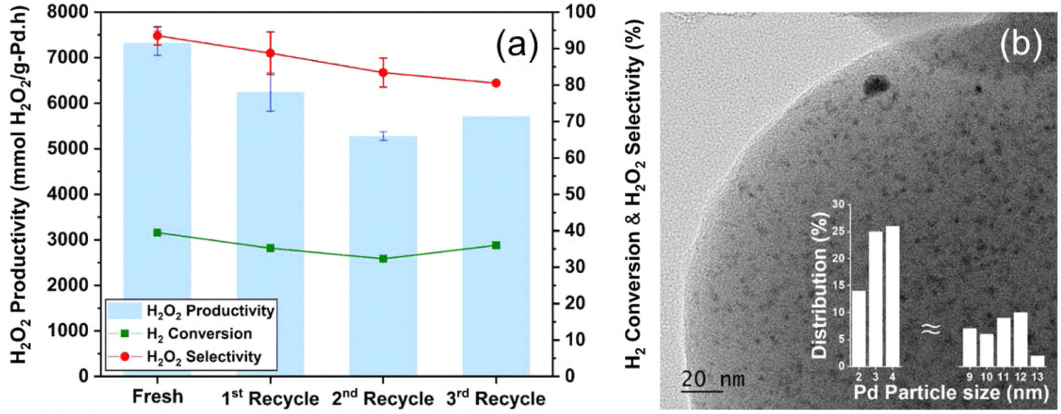

Fig. 11. (a) Recycle test of Pd/$CN_{0.8}$ catalyst and (b) TEM image of the recycled catalyst. Reaction conditions: catalyst (20 mg), $N_2/H_2/O_2$ (mol%)=3.8/5.0/91.2 (30 bar), total gas flow rate=40 mL/min, 60 wt% methanol/water solvent (26 g), 275 K, 1 h.

from 39% (fresh) to 35–36% over the 1st–3rd recycle runs without a pronounced loss of activity. In contrast, the H_2O_2 selectivity gradually declines with increasing recycle number, from 94% to 81%, accompanied by an overall decrease in H_2O_2 productivity from 7323 to 5711 mmol H_2O_2/g-Pd·h. This behavior can be interpreted together with the TEM results of the recycled catalyst (Fig. 12(b)). A minor population of larger Pd NPs (~9–13 nm) is observed in the particle size distribution, suggesting limited particle growth/aggregation during reuse. Overall, the slight increase in Pd NP size distribution upon recycling is consistent with the gradual decrease in H_2O_2 selectivity and productivity.

4. Conclusions

This study shows that glucose-derived N-doped porous carbons prepared by K_2CO_3/KCl activation are effective supports for Pd catalysts, enabling efficient DSHP reaction without corrosive additives. Nitrogen doping increased surface area and generated pyridinic/pyrrolic functionalities that strengthened metal-support interactions, improved Pd dispersion, and maintained small Pd domains compared with undoped carbon. XPS indicates that Pd sites exist as mixed Pd^{2+}/Pd^0 surfaces, and catalytic performance correlates more strongly with H_2O_2 selectivity than with H_2 conversion. The DSHP performance of Pd/CN_x catalysts strongly depends on the N-doping level, and the best performance was achieved over Pd/$CN_{0.8}$, providing an H_2O_2 selectivity of 91% and a productivity of 7056 mmol H_2O_2/g-Pd·h. In contrast, excessive N content ($CN_{1.4}$-$CN_{8.5}$) caused rapid H_2O_2 loss through hydrogenation and decomposition, leading to severe drops in selectivity and productivity. Recycling tests showed stable conversion but gradual selectivity/productivity decay, consistent with limited Pd growth during reuse. Overall, fine control of N content/speciation and the resulting Pd dispersion and Pd^{2+}/Pd^0 balance is important for suppressing non-selective pathways and improving DSHP performance.

Declaration of Competing Interest

The authors declare that they have no known competing financial interests or personal relationships that could have appeared to influence the work reported in this paper.

Acknowledgment

This research was supported by Basic Science Research Program through the National Research Foundation of Korea (NRF) funded by the Ministry of Education (RS-2016-NR018630).

References

1. Campos-Martin, J. M., Blanco-Brieva, G. and Fierro, J. L. G., "Hydrogen Peroxide Synthesis: An Outlook Beyond the Anthraquinone Process," *Angew. Chem. Int. Ed.*, **45**, 6962-6984(2006).
2. Yi, Y., Wang, L., Li, G. and Guo, H., "A Review on Research Progress in the Direct Synthesis of Hydrogen Peroxide From Hydrogen and Oxygen: Noble-metal Catalytic Method, Fuel-cell Method and Plasma Method," *Catal. Sci. Technol.*, **6**, 1593-1610(2016).
3. Samanta, C., "Direct Synthesis of Hydrogen Peroxide From Hydrogen and Oxygen: An Overview of Recent Developments in the Process," *Appl. Catal. A: Gen.*, **350**, 133-149(2008).
4. Dittmeyer, R., Grunwaldt, J. D. and Pashkova, A., "A Review of Catalyst Performance and Novel Reaction Engineering Concepts in Direct Synthesis of Hydrogen Peroxide," *Catal. Today*, **248**, 149-159(2015).
5. Chen, L., Medlin, J. W. and Grönbeck, H., "On the Reaction Mechanism of Direct H_2O_2 Formation over Pd Catalysts," *ACS Catal.*, **11**, 2735-2745(2021).
6. Lee, S., Jeong, H. and Chung, Y.-M., "Direct Synthesis of Hydrogen Peroxide over Pd/C Catalyst Prepared by Selective Adsorption Deposition Method," *J. Catal.*, **365**, 125-137(2018).
7. Lunsford, J. H., "The Direct Formation of H_2O_2 from H_2 and O_2 over Palladium Catalysts," *J. Catal.*, **216**, 455-460(2003).
8. Dissanayake, D. P. and Lunsford, J. H., "Evidence for the Role of Colloidal Palladium in the Catalytic Formation of H_2O_2 from H_2 and O_2," *J. Catal.*, **206**, 173-176(2002).
9. Choudhary, V. R., Samanta, C. and Choudhary, T. V., "Direct Oxidation of H_2 to H_2O_2 over Pd-based Catalysts: Influence of Oxidation State, Support and Metal Additives," *Appl. Catal. A: Gen.*, **308**, 128-133(2006).
10. Choudhary, V. R., Samanta, C. and Choudhary, T. V., "Factors Influencing Decomposition of H_2O_2 over Supported Pd Catalyst in Aqueous Medium," *J. Mol. Catal. A: Chem.*, **260**, 115-120(2006).
11. Choudhary, V. R., Samanta, C. and Jana, P., "Formation from Direct Oxidation of H_2 and Destruction by Decomposition/hydrogenation of H_2O_2 over Pd/C Catalyst in Aqueous Medium Containing Different Acids and Halide Anions," *Appl. Catal. A: Gen.*, **317**, 234-243(2007).
12. Choudhary, V. R., Samanta, C. and Gaikwad, A. G., "Drastic Increase of Selectivity for H_2O_2 Formation in Direct Oxidation of H_2 to H_2O_2 over Supported Pd Catalysts Due to Their Bromination," *Chem. Commun.*, 2054-2055(2004).
13. Lewis, R. J., Edwards, J. K., Freakley, S. J. and Hutchings, G. J., "Solid Acid Additives as Recoverable Promoters for the Direct Synthesis of Hydrogen Peroxide," *Ind. Eng. Chem. Res.*, **56**, 13287-13293(2017).
14. Auer, E., Freund, A., Pietsch, J. and Tacke, T., "Carbons as Supports for Industrial Precious Metal Catalysts," *Appl. Catal. A: Gen.*, **173**, 259-271(1998).
15. Edwards, J. K., Solsona, B., Carley, A. F., Herzing, A. A., Kiely, C. J. and Hutchings, G. J., "Switching off Hydrogen Peroxide Hydrogenation in the Direct Synthesis Process," *Science*, **323**, 1037-1041(2009).
16. Freakley, S. J., He, Q., Harrhy, J. H., Lu, L., Morgan, D. J. et al., "Palladium-tin Catalysts for the Direct Synthesis of H_2O_2 with High Selectivity," *Science*, **351**, 961-965(2016).
17. Tian, P., Xu, X., Ao, C., Ding, D., Li, W. et al., "Direct and Selective Synthesis of Hydrogen Peroxide over Palladium–tellurium Catalysts at Ambient Pressure," *ChemSusChem*, **10**, 3342-3346(2017).
18. Arrigo, R., Schuster, M. E., Abate, S., Giorgianni, G. et al., "Pd Supported on Carbon Nitride Boosts the Direct Hydrogen Peroxide Synthesis," *ACS Catal.*, **6**, 6959-6966(2016).
19. Arrigo, R., Schuster, M. E., Abate, S., Wrabetz, S. et al., "Dynamics of Palladium on Nanocarbon in the Direct Synthesis of H_2O_2," *ChemSusChem*, **7**, 179-194(2014).
20. Ye, Y., Chun, J., Park, S., Kim, T. J., Chung, Y. M., Oh, S. H., Song, I. K. and Lee, J., "A Study of the Palladium Size Effect on the Direct Synthesis of Hydrogen Peroxide from Hydrogen and Oxygen Using Highly Uniform Palladium Nanoparticles Supported on Carbon," *Korean J. Chem. Eng.*, **29**, 1115-1118(2012).
21. Edwards, J. K., Freakley, S. J., Lewis, R. J., Pritchard, J. C. and Hutchings, G. J., "Advances in the Direct Synthesis of Hydrogen Peroxide from Hydrogen and Oxygen," *Catal. Today*, **248**, 3-9 (2015).
22. Sun, M., Zhang, J., Zhang, Q., Wang, Y. and Wan, H., "Polyoxometalate-supported Pd Nanoparticles as Efficient Catalysts for the Direct Synthesis of Hydrogen Peroxide in the Absence of Acid or Halide Promoters," *Chem. Commun.*, 5174-5176(2009).
23. Jiang, D., Shi, Y., Zhou, L. and Ma, J., "Promotional Effect of Nitrogen-doped and Pore Structure for the Direct Synthesis of Hydrogen Peroxide from Hydrogen and Oxygen by Pd/C Catalyst at Ambient Pressure," *Arab. J. Chem.*, **16**, 104452(2023).
24. Biasi, P., Sterchele, S., Bizzotto, F., Manzoli, M., Lindholm, S., Ek, P., Bobacka, J., Mikkola, J. P. and Salmi, T., "Application of the Catalyst Wet Pretreatment Method (CWPM) for Catalytic Direct Synthesis of H_2O_2," *Catal. Today*, **246**, 207-215(2015).
25. Zhang, Y., Pan, H., Murugananthan, M. and Sun, P., "Glucose and Melamine Derived Nitrogen-doped Carbonaceous Catalyst for Nonradical Peroxymonosulfate Activation," *Carbon*, **156**, 399-409(2020).
26. Seredych, M., Biggs, M. J. and Bandosz, T. J., "Oxygen Reduction on Chemically Heterogeneous Iron-containing Nanoporous Carbon: The Effects of Specific Surface Functionalities," *Microporous Mesoporous Mater.*, **221**, 137-149(2015).
27. Zborowski, K. K. and Poater, J., "Pyrrole and Pyridine in the Water Environment: Effect of Discrete and Continuum Solvation Models," *ACS Omega*, **6**, 24693-24699(2021).
28. Fuertes, A. B., Ferrero, G. A., Diez, N. and Sevilla, M., "A Green Route to High-surface-area Carbons by Chemical Activation of Biomass-based Products with Sodium Thiosulfate," *ACS Sustain. Chem. Eng.*, **6**, 16323-16331(2018).
29. Sevilla, M., Díez, N. and Fuertes, A. B., "More Sustainable Chemical Activation Strategies for the Production of Porous Carbons," *ChemSusChem*, **14**, 94-117(2021).
30. Titirici, M. M. and Antonietti, M., "Chemistry and Materials Options of Sustainable Carbon Materials Made by Hydrothermal Carbonization," *Chem. Soc. Rev.*, **39**, 103-116(2010).

31. Lee, H., Kim, S., Lee, D. W. and Lee, K. Y., "Direct synthesis of Hydrogen Peroxide from Hydrogen and Oxygen over a Pd Core–silica Shell Catalyst," *Catal. Commun.*, **12**, 968-971(2011).
32. Vu, H. T. T., Vo, V. L. N. and Chung, Y. M., "Geometric, Electronic, and Synergistic Effect in the Sulfonated Carbon-supported Pd Catalysts for the Direct Synthesis of Hydrogen Peroxide," *Appl. Catal. A: Gen.*, **607**, 117867(2020).

Authors

Young-Min Chung: Professor, Department of Chemical Engineering, Kunsan National University, 558 Daehak-ro, Gunsan, Jeollabuk-Do 54150, Republic of Korea; ymchung@kunsan.ac.kr

Seung-Yeol Oh: Graduate student, Department of Chemical Engineering, Kunsan National University, 558 Daehak-ro, Gunsan, Jeollabuk-Do 54150, Republic of Korea; ohseungyeol@kunsan.ac.kr

Na-Yeong Ahn: Graduate student, Department of Chemical Engineering, Kunsan National University, 558 Daehak-ro, Gunsan, Jeollabuk-Do 54150, Republic of Korea; anna2345@kunsan.ac.kr